Theoretical study of X_4N (X=Sc and Y) antiperovskite by first principle calculations and Monte Carlo simulationone column format

Soukaina Bouhmaidi[1*], *Abdelouahid* Azouaoui[2], *Redi Kristian* Pingakand[3] , *Najib* Benzakour[2], and *Larbi* Setti[1]

[1]TED Team, FPL, Abdelmalek Essaadi University, Tetouan, Morocco.
[2]LSP, FS, Sidi Mohamed Ben Abdellah University, Fez, Morocco.
[3]DP, FSE, University of Nusa Cendana, Kupang, Nusa Tenggara Timur, Indonesia.

Abstract. The structural, electronic, magnetic and elastic properties of X_4N (X=Sc and Y) have been investigated in the framework of density functional theory (DFT) and Monte Carlo simulation (MC). The obtained results indicated that X4N exhibits a metallic behaviour, Sc_4N is stable in ferromagnetic configuration with a total magnetic moment of 2.26μB while Y_4N is stable in nonmagnetic configuration. The elastic constants and their derived parameters are studied and the results showed that these compounds are ductile. The Monte Carlo simulation was used to investigate the magnetic properties of Sc_4N including the thermal magnetization and susceptibility. Moreover, the transition temperature TC, hysteresis cycle, coercive field and remanent magnetization are presented. The results also revealed that Sc_4N Sc_4N a ferromagnetic-to-paramagnetic transition at two different conditions, i.e. at 10 GPa and at temperature of 30 K.

1 Introduction

Transition metals nitrides (TMN) have attracted a great deal of interest because of their excellent properties such as high hardness, high mechanical resistance and high melting temperature [1,2]. For this reason, these materials have been used in a various potential application in the industry such as magnetic recording, microwave-absorbing materials and optical and anticorrosion coatings [3–5].
Two main groups characterize these materials: Transition metals mononitrides (TMN) and tetra transition metals nitrides (TM_4N). Most TMN materials crystallize in two structures, rock salt (NaCl) [6] and zincblende (ZB) [7] and all these compounds show metallic behaviour except ScN and YN, which are semiconductors with a narrow indirect bandgap [8]. On the other hand, the TM_4N crystallize in the antiperovskite structure, showing metallic behavior and possessing various magnetic properties: Mn_4N is ferrimagnetic with low magnetic moment [9, 10], Fe_4N and Co_4N are ferromagnetic with high magnetic moment and Cu_4N are nonmagnetic [11,12].

* Corresponding author: author@email.org

Meinert [13] used density functional theory combined with Monte Carlo simulations to evaluate exchange interactions and estimate the critical temperatures of five tetra-transition-metal nitrides, namely Cr_4N, Mn_4N, Fe_4N, Co_4N, and Ni_4N. The predicted values were generally consistent with the available experimental measurements, particularly for Fe_4N and Mn_4N. In contrast, the antiperovskite nitrides Sc_4N and Y_4N have received considerably less attention than other members of the TM_4N family.

In the present study, first-principles calculations within the DFT framework and the GGA approximation were carried out to determine the structural, electronic, magnetic, and elastic characteristics of X_4N, where X represents Sc or Y. The parameters obtained from the DFT calculations were subsequently introduced into an Ising-model Monte Carlo simulation to examine the temperature-dependent magnetization, magnetic susceptibility, hysteresis behaviour, and Curie temperature of Sc_4N. Because experimental measurements for these compounds are currently unavailable, the calculated properties were assessed through comparison with related antiperovskite nitrides, including Mn_4N, Cr_4N, and Co_4N. Consequently, the present findings constitute useful theoretical predictions and may serve as reference data for future experimental investigations of Sc_4N and Y_4N.

2 Method of calculations

Computations of structural, electronic, magnetic and elastic properties of X_4N (X=Sc and Y) were performed using density functional theory (DFT) approach implemented in the QUANTUM ESPRESSO package [14,15]. The exchange–correlation functional was evaluated using the generalized gradient approximation (GGA) suggested by Perdew, Burke, and Ernzerhof (PBE) [15]. The electron-ion interactions were treated using the Vanderbilt ultrasoft pseudopotentials [7] with the valence electrons for Sc ($3d^14s^2$), Y ($4d^15s^2$) and N($2s^22p^3$). A plane-wave kinetic-energy cutoff of 520 eV was adopted, while the charge-density cutoff was set to eight times this value. The Monkhorst-Pack scheme [11] with a special k-points grid of 8 × 8 × 8 was used to sample the Brillouin zone. We chose the Methfessel-Paxton scheme [9] for the Fermi level smearing and the corresponding smearing parameter equals 0.01 eV.

All calculations based on DFT were performed at the equilibrium lattice parameter. The thermo−pw package [10] was used to study the elastic and thermodynamic properties in the range of temperature from 0K to 800K. These properties were calculated and presented using the Voigt-Reuss-Hill approximation [11].

3 Results and discussion

3.1 Structural properties

The X_4N antiperovskites (X = Sc or Y) adopt a **primitive cubic structure** with space group $Pm\bar{3}m$, No. 221. Their unit cell consists of five atoms: one nitrogen atom and four X atoms. The X atoms occupy two nonequivalent crystallographic sites, with one effective atom located at the cube corners (Xc) and three atoms positioned at the face centres (Xf), while nitrogen occupies the body-centred site. The corresponding Wyckoff sites and atomic coordinates are provided in Fig. 1 and Table 1.

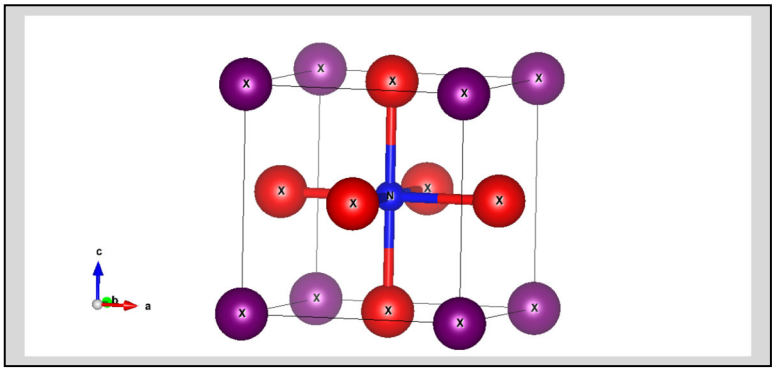

Fig. 1. The antiperovskite crystal structure of X_4N.

Table 1. Wyckoff parameters for each atom of X_4N in antiperovskite structure.

atom	wyckoff site	x	y	z
Xc	1a	0	0	0
N	1b	0.5	0.5	0.5
Xa	3c	1/2	1/2	0

To determine the equilibrium structural parameters, the total energy of X_4N was calculated as a function of the lattice constant for both ferromagnetic (FM) and nonmagnetic (NM) states. The resulting energy curves, displayed in Fig. 2, were fitted using the Murnaghan equation of state [14]. The equilibrium lattice parameter was identified from the minimum of each fitted curve.

The chemical stability of the compounds was then evaluated through their formation energy per atom. When bulk X and molecular nitrogen are taken as the reference states, the formation energy is expressed as:

$$E_f = \frac{E_{tot}^{X_4N} - E_{bulk}^{X} - E_{bulk}^{N}}{5} \quad (1)$$

Where $E_{tot}^{X_4N}$ denotes the total energy of the X4N bulk, E_{bulk}^{X} is the energy per atom of the elemental transition metal X, and E_{bulk}^{N} represents the total energy of an isolated nitrogen molecule. The optimized lattice constants, total magnetic moments, and calculated formation energies are reported in Table 2.The obtained values of lattice parameters, total magnetic moment and formation energies are summarized in Table 2.

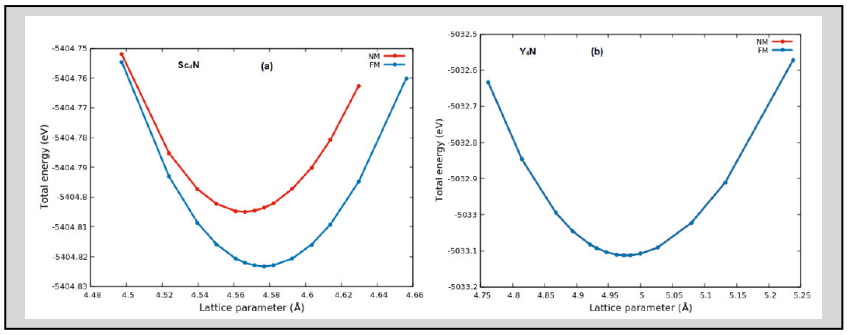

Fig. 2. Total energy as a function of lattice parameter for X_4N.

Table 2. Configuration, lattice parameter (in Å), total magnetic moment (in μ_B) and the formation energy (in eV) of X_4N.

Compound	configuration	a(Å)	m(μ_B)	E_f
Sc_4N	FM	4.57	2.26	-3.84
	NM	4.56	-	-3.82
	[11]	4.58	2.24	-3.09
	[25]	4.555	0.0	-2.98
Y_4N	FM	4.97	0.0	-3.307
	NM	4.97	0.0	-3.306
	[11]	4.98	0.0	-2.67

From Table 2, it is found that the obtained results are in good agreement with the theoretical available works [11,15]. These results show that Sc_4N is stable in FM configuration with the value of lattice parameter about 4.57Å and total magnetic moment about $2.26\mu_B$. In the case of Y_4N, we have found the same value of lattice parameter for FM and NM configurations with the total magnetic moment equal to zero. For this reason, the NM configuration is the most stable. The E_f values of X_4N (X=Sc, Y) are negative (see Table 2),
which means that they are chemically stable in antiperovskite structure. It is noticed that the obtained values of Ef for X4N are higher than those of the similar compounds, Mn_4N (-1.78 eV) [10], Cr_4N (-0.698 eV) [6] and Co4N (0.082 eV) [12]. These values indicate that Sc_4N and Y_4N are more stable in the antiperovskite structure than other similar compounds.

From Fig.2a, we can see that when the lattice parameter increases the energy difference increases. In this way, we have computed the total magnetic moment as a function of pressure to find the transition pressure between the FM and NM configuration and the obtained results are depicted in Fig.3.

Our results show that the magnetic moment of *Sc*4*N* is vanished at the pressure of about 10GPa, which means that *Sc*4*N* experiences a transition from FM configuration to NM at the critical pressure $pc = 10GPa$.

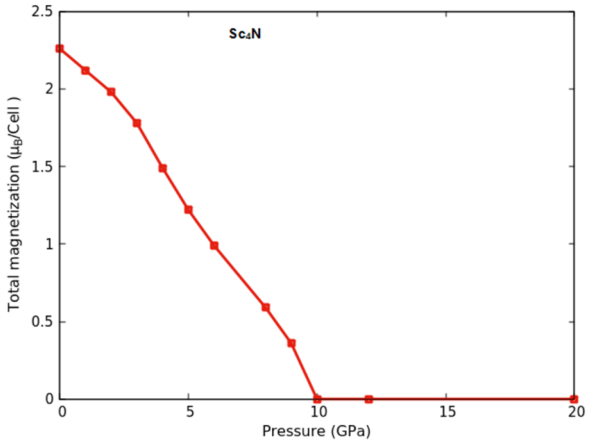

Fig. 3. Total magnetization as a function of pressure of *Sc4N*.

3.2 Electronic properties of *X4N*

The calculated energy bands structures and density of states (DOS) for cubic antiperovskite X_4N (X=Sc and Y) at the equilibrium lattice parameter are presented in Fig.4. In these figures the X and N atoms are represented by the contribution of 3d and 2p orbitals.

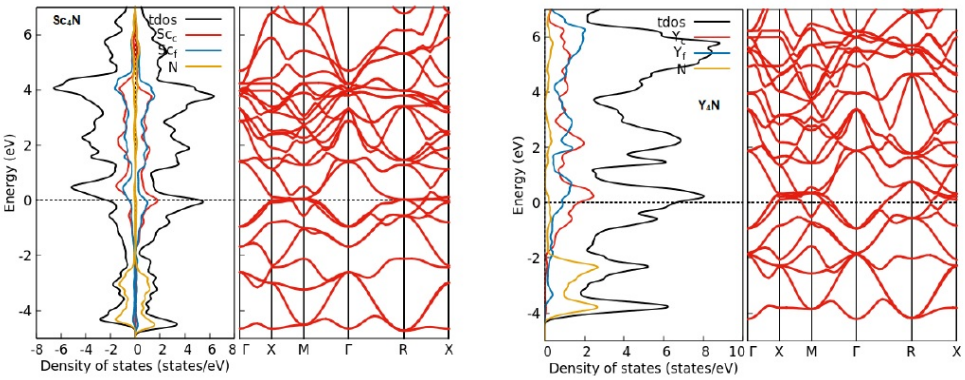

Fig. 4. Band structure, total and partial density of state of X_4N.

The zero energy in these figures indicates the Fermi level presented by dashed horizontal line. The densities of state and band structures show that the compounds have metallic behavior because no band gap observed. These results confirm the same metallic behavior for other similar transition metal nitrides [6, 11, 12]. This behavior is due to the strong hybridization of 2p orbitals of N atom and 3d orbitals of X (Sc and Y).

3.3 Elastic properties of *X4N*

The elastic response of a material is essential for assessing its mechanical stability and potential technological applications. Owing to the cubic symmetry of Sc_4N and Y_4N, their elastic behaviour is fully described by three independent constants: (C_{11}, (C_{12}), and (C_{44}). The calculated elastic constants of both antiperovskite compounds are reported in Table together with previously published theoretical values for comparison.

Table 3. Calculated elastic constants Cij (GPa) of X4N..

X4N	**C_{11}**	**C_{12}**	**C_{44}**
Sc_4N	106.3	69.67	48.96
[11]	111.2	70.3	49.9
Y_4N	89.93	52.68	41.52
[11]	87.7	55.5	39.7

The mechanical stability of *X*4*N* (X=Sc and Y) is determined by the following equations:

$$C_{11} + 2C_{12} > 0 \quad (2)$$

$$C_{11} - C_{12} > 0 \quad (3)$$

$$C_{44} > 0 \quad (4)$$

$$C_{12} < B < C_{11} \quad (5)$$

The obtained values agree well with that obtained in Ref. [11] and completely satisfy the Born-Huang criteria [6]. Hence X_4N (X=Sc and Y) compounds are mechanically stable. We can note that the obtained values of C_{ij} for Sc_4N and Y_4N are lower than those obtained in other similar structures such as Mn_4N, Cr_4N, Co_4N [6,11,12], which indicates that Sc_4N and Y_4N possesses a lower hardness compared to other compounds listed above. Besides, it can be concluded from the computed values of C_{ij} , that C_{11} is significantly larger than C_{12} and C_{44}, which means that the Sc_4N and Y_4N are less incompressible if some pressure is applied along the x-direction. These constants are very crucial and allow one to obtain several mechanical properties such as the bulk modulus (B), shear modulus (G), Young's modulus (E), and Poisson's ratio (υ) by using the following expressions:

$$B = \frac{1}{2}(B_R + B_V) \quad (6)$$

$$G = \frac{1}{2}(G_R + G_V) \quad (7)$$

Here, (G_V) and (G_R) represent the Voigt and Reuss shear moduli, respectively, whereas (B_V) and (B_R) denote the corresponding bulk moduli.

$$E = \frac{9BG}{3B+G} \quad (8)$$

$$\upsilon = \frac{3B-2G}{2(3B+G)} \quad (9)$$

Table 4. Calculated bulk modulus B (GPa), Shear modulus G (GPa), Young's modulus E (GPa), Pugh's ratio (k), Vickers hardness *HV* (GPa), Poisson's ratio (υ), Debye θ_D and melting T_m temperatures (K) of X_4N (X=Sc, N).

	B	**G**	**E**	**k**	**H_V**	**υ**	**θ_D**	**Tm**
Sc_4N	81.88	87.20	33.01	0.4	3.89	0.32	384.8	1181 K
[11]	**83.9**	91.9	34.9	0.42	4.2	0.32	400.5	-
Y4N	65.96	78.18	30.10	0.46	4.18	0.3	277.8	1084 K
[11]	66.3	72.8	27.6	0.42	3.6	0.32	269.1	-

In order to confirm the ductile or brittle behavior of these compounds, we have calculated the Pugh's ratio (k=G/B) and Cauchy pressure ($Cp = C_{12} - C_{44}$). The condition of material ductility is given by Pettifor [27] ($C_p \geq 0$) and Pugh [28] ($k \leq 0.57$). With these conditions, we observe that both compounds possess a ductile behavior. The values of Poisson's ratio

are equal to 0.32 and 0.3 for Sc_4N and Y_4N, respectively, which means that our compounds present a metallic bonding.

To study the hardness of these compounds, we have computed the Vickers hardness (H_V) using Tian's model [9] with the following equation:

$$H_V = 0.92k^{1.137}G^{0.708} \tag{10}$$

The values of H_V for Sc_4N and Y_4N are 3.89 GPa and 4.18 GPa, respectively. These values are less than 10 GPa, which means that these compounds are not very hard. The Debye temperature θ_D is one of the most important parameters that describes the thermal properties of materials given by the following equation:

$$\theta_D = \frac{h}{k_B}\left[\frac{3n}{4\pi}\left(\frac{N_A\times\rho}{M}\right)\right]^{1/3} \upsilon_m \tag{11}$$

where h is Planck's constant, k_B is Boltzmann's constant, N_A is Avogadro's number, ρ is the density of the material, M is the molecular weight of the primitive cell and n is the number of atoms in the cell. The speed of sound υ_m is given by:

$$\upsilon_m = \left[\frac{2}{\upsilon_t^3} + \frac{3}{\upsilon_l^3}\right]^{1/3} \tag{12}$$

where, υ_l and υ_t are the longitudinal and transverse sound speeds, respectively, and they are determined from the bulk (B) and shear (G) modulus by the following expressions [10].

$$\upsilon_t = \left(\frac{G}{\rho}\right)^{1/2}, \quad \upsilon_l = \left(\frac{3B+4G}{3\rho}\right)^{1/2} \tag{13}$$

Another most important parameter, melting temperature T_m has been computed by the following equation [11]:

$$T_m = [553 + 5.911 \times C_{12}](GPa) \pm 300$$

The obtained values of Debye and melting temperatures are listed in Table 4. The value of θ_D for Sc_4N and Y_4N are found to be equal to 384.8K and 277.8K respectively. Sc_4N presents a high value of θ_D and T_m than Y_4N.

Fig.5 presents the thermal variation of entropy of X4N in the range 0 to 800K. It is found that the entropy increases with temperature and at low temperature the entropy of Sc_4N is greater than Y_4N and at high temperatures the entropy of Y_4N becomes higher than that of Sc_4N .

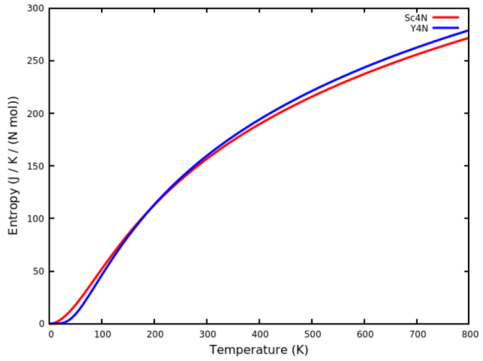

Fig. 5. The entropy of *X4N* compounds as a function of temperature.

It is known that the heat capacity (*Cv*) provides valuable information about the lattice vibrations of a material. We illustrate in Fig.6 the *Cv* of X_4N. From this figure, we can see the sharp increase of *Cv* up to 200K and then its increment raises slowly. However, at low temperatures *Cv* follows *T*3 law. Above this temperature, *Cv* tends towards the Dulong-Petit limit, meaning that the total phonon modes in these systems are fully excited. From this figure, we can see that the *Cv* present almost the same variation for both compounds.

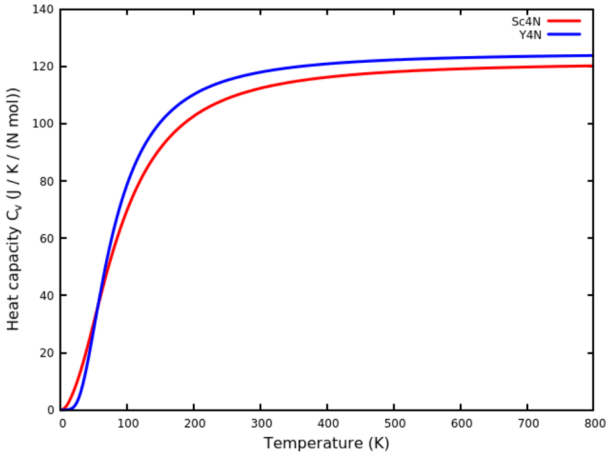

Fig. 6. The heat capacity at constant volume (*Cv*) with temperature for *X*4*N*.

To complete this part, we have studied the dynamical stability of the X_4N (X=Sc and Y) compounds by calculating its phonon dispersion along high symmetry directions in the first Brillouin zone, and density of phonon states. The obtained results are presented in Fig. 7. For Sc_4N, the frequencies of phonon modes observed are positive and negative, which show that this material is dynamically unstable in antiperovskite structure. For Y_4N, the frequencies of phonon modes observed are positive and we do not observe any phonon anomaly in the density of phonon states, which shows that this material is dynamically stable in antiperovskite structure. From these figures, we can see that there is no gap separating the acoustic and optical branches due to a large difference between the masses of X (Sc, Y) and N.

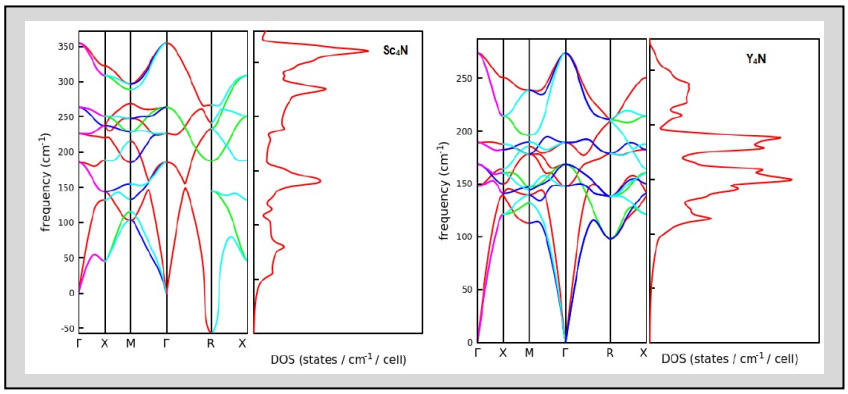

Fig. 7. Phonon dispersion and density of phonon states of *X*4*N*.

3.4 Monte Carlo simulation of *Sc4N*

The Hamiltonian of the studied compound Sc_4N with a ferromagnetic configuration including the nearest neighbors interactions and an external magnetic field (H_{ext}) is given by:

$$H = J_1 \sum_{<ij>} S_i S_j - H_{ext} \sum_i S_i \quad (14)$$

where $< ij >$ stands for the first nearest neighbor spins (i and j) and J_1 is the exchange interactions between the first nearest neighbor magnetic atoms with the spins s. The Monte Carlo simulations are used to study the magnetic properties such as thermal magnetization, susceptibility and hysteresis loop of *Sc4N* under the Metropolis algorithm. In this work, we have used the periodic boundary conditions and for more details about Monte Carlo simulations are used in previous work [6,12]. Our program calculates the following quantities:

The total magnetization is given by:

$$M = \frac{1}{N} < \sum_i S_i > \quad (15)$$

$$\chi = \beta(< M^2 > - < M >^2) \quad (16)$$

Where $\beta = \frac{1}{k_B T}$ and T denotes the absolute temperature.

To calculate the exchange parameter J_1 with first principles calculations, we have used the expression:

$$\frac{J_1}{k_B} = \frac{E_{NM} - E_{FM}}{2zs(s+1)} \quad (17)$$

Where E_{NM} and E_{FM} are the total energy of nonmagnetic and ferromagnetic configurations, respectively. z is the number of first nearest neighbors around Sc atom (z=12). The Curie temperature (T_C^{MFT}) can be expressed in the mean field theory approximation (MFT) by:

$$k_B T_C^{MFT} = \frac{2}{3} J_1 \quad (18)$$

In this work, the sum extends over all the first neighbor atoms. From equations 17 and 18, T_C^{DFT} can be given by the following formula:

$$k_B T_C^{DFT} = \frac{E_{NM} - E_{FM}}{6k_B} \quad (19)$$

The predictive values of J_1 , T_C^{MFT} , T_C^{DFT} and T_C^{MC} are presented in Table 5. The magnetic susceptibility of Sc_4N is presented in Fig.8. According to this figure, the total susceptibility has a peak corresponding to a transition temperature value of about T_C = 30K. This value is very low compared to those obtained for similar compounds Mn_4N(705K) [10], Cr_4N (295K) [6] and Co_4N(820K) [12].

The effect of varying the external field on the behavior of magnetization of *Sc4N* is illustrated in Figs.9(a-b). We can see that the increase of *Hext* leads to an increase in Curie temperature. *TC* deduced from the maximum of magnetic susceptibilites in Fig.9b.

We have presented in Fig.10 the magnetic hysteresis cycle for three temperatures T=20K, 25K and 30K. We can see that the surface loop decreases sharply with increasing temperature, coercive field and magnetization remanent are also decreased. The effect of temperature on the hysteresis cycle leads to a decrease in the coercive field, magnetization remanent and saturation.

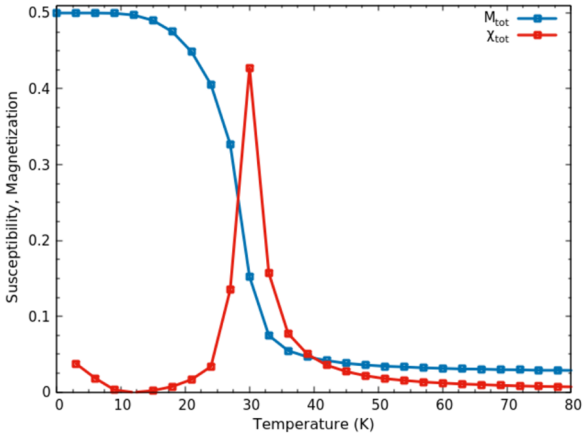

Fig. 8. The Total magnetization and susceptibility as a function of temperature of *Sc*4*N* for *Hext* = 0.

Table 5. The exchange parameter J_1 and Curie temperatures T_C of Sc_4N for $H_{ext} = 0$.

J_1(meV)	18.5
T_C^{MFT}(K)	71.5
T_C^{DFT}(K)	35.94
T_C^{MC}(K)	30

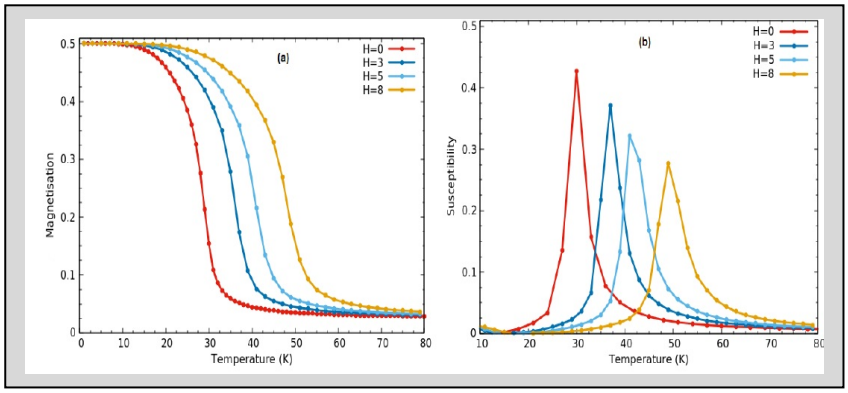

Fig. 9. (a) The total magnetization, (b) The magnetic susceptibility of Sc_4N as a function of temperature for different value of H_{ext}.

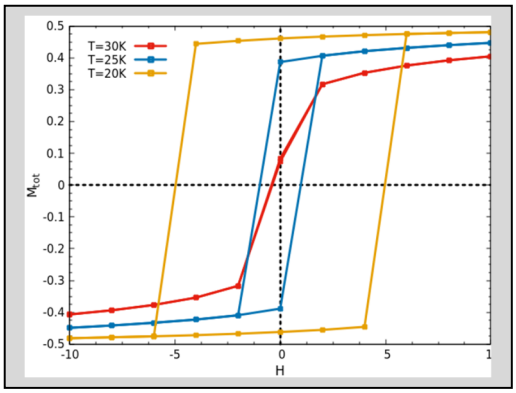

Fig. 10. The magnetic hysteresis cycle of *Sc*4*N* at 20K, 25K and 30K.

4 Conclusion

In this paper, we have studied the structural, electronic, elastic and magnetic properties of the X_4N (X=Sc and Y) using the density functional theory and Monte Carlo simulation. The obtained results showed that X_4N are chemically stable in antiperovskite structure and exhibit a metallic behavior. Sc_4N is stable in ferromagnetic configuration with a total magnetic moment of 2.26 μ_B and presents a transition under pressure at 10GPa from ferromagnetic to nonmagnetic phase whereas Y_4N is stable in nonmagnetic configuration. The study of elastic constants and their derived parameters indicated that Sc_4N and Y_4N are mechanically stable, ductile and have a metallic bond. The Monte Carlo simulation was used to investigate the magnetic properties of Sc_4N such as thermal magnetization and susceptibility. The MC simulation revealed that Sc_4N exhibits a transition under temperature at $T_C = 30K$ from ferromagnetic to nonmagnetic phase and T_C increases with the increase of external field. Furthermore, the hysteresis cycle, coercive field, and remanent magnetization are found to decrease with increasing temperature.

References

1. R. Wuhrer, W.Y. Yeung, A comparative study of magnetron co-sputtered nanocrystalline titanium aluminium and chromium aluminium nitride coatings, Scripta Materialia, **50**,1461 (2004).
2. A. Anzai, T. Gushi, T. Komori, S. Honda, S. Isogami, T. Suemasu, Transition from minority to majority spin transport in iron-manganese nitride Fe4−xMnxN films with increasing x, Journal of Applied Physics, **124**, 123905 (2018).
3. A.I. Linnik, A.M. Prudnikov, R.V. Shalaev, T.A. Linnik, V.N. Varyukhin, S.A. Kostyrya, V.V. Burkhovetskii, Magnetic properties and thermal modification of nanostructured films of nickel nitrides Technical Physics Letters, **39**, 143 (2013).
4. P.R. Cantwell, U.J. Gibson, D.A. Allwood, H. Macleod, Optical coatings for improved contrast in longitudinal magneto-optic Kerr effect measurements, Journal of applied physics, **100**, 093910 (2006).
5. A Azouaoui, N Benzakour, A Hourmatallah, K Bouslykhane, Structural and Magnetic Properties of CrN: Investigated by First-Principles Calculations, Monte Carlo Simulation, and High-Temperature Series Expansions, Journal of Superconductivity and Novel Magnetism, **33**, 3113 (2020)

6. C. Stampfl, W. Mannstadt, R. Asahi, A.J. Freeman, Electronic structure and physical properties of early transition metal mononitrides: Density-functional theory LDA, GGA, and screened-exchange LDA FLAPW calculations, Physical Review B, **63**, 155106 (2001).
7. Markus Meinert, Exchange interactions and Curie temperatures of the tetrametal nitrides Cr4N, Mn4N, Fe4N, Co4N, and Ni4N, Journal of Physics Condensed Matter, **28**, 056006 (2016).
8. A. Reuss, Calculation of the Flow Limits of Mixed Crystals on the Basis of the Plasticity of Monocrystals, Journal of Applied Mathematics and Mechanics, **9**, 49 (1929).
9. R. Hill, The Elastic **Behaviour** of a Crystalline Aggregate, Proceedings of the Physical Society. Section A, 65, 349 (1952).
10. F.D. Murnaghan, The Compressibility of Media under Extreme Pressures, Proceedings of the national academy of sciences of the United States of America, **30**, 244 (1944).
11. A. Azouaoui, N. Benzakour, A. Hourmatallah, K. Bouslykhane, tructural and Magnetic Properties of Co-Zn Ferrites: Density functional theory calculations and High-temperature series expansions, Journal of Superconductivity and Novel Magnetism, pages 1, (2020).
12. R. K. Pingak, A. Harbi, F. Nitti, S. Bouhmaidi, D. Tambaru, A. Z. Johannes, N. U.J. Hauwali, Abdul Wahid, M. Moutaabbid, L. Setti,The incorporation of Cs and K into the crystal structure of Rb2SnBr6 double perovskite: A DFT perspective, Materials Science in Semiconductor Processing, **186**, 109044 (2025).
13. J. W. Wafula, G. S. Manyali, J. W. Makokha, Y. Madallah, S. Bouhmaidi, L. Setti,
14. DFT+U investigation of electronic, optical, and thermoelectric properties of YAuX (X=Si or Ge or Sn) half-Heusler alloys, Results in Physics, **61**, 107747 (2024).
15. R. K. Pingak, A. Harbi, S. Bouhmaidi, F. Nitti, M. Moutaabbid, L. Setti, A.Z. Johannes, N. U. J. Hauwali, Vacancy-ordered CsRbGeCl6 and CsRbGeBr6 perovskites as new promising non-toxic materials for photovoltaic applications: A DFT investigation, Chemical Physics, **584**, 112348 (2024).